The Journal of Chemical Physics

NH_2^- in a cold ion trap with He buffer gas: *Ab initio* quantum modeling of the interaction potential and of state-changing multichannel dynamics

Cite as: J. Chem. Phys. **148**, 184305 (2018); https://doi.org/10.1063/1.5022633
Submitted: 17 January 2018 . Accepted: 20 April 2018 . Published Online: 09 May 2018

Mario Hernández Vera, Ersin Yurtsever, Roland Wester, and Franco A. Gianturco

View Online Export Citation CrossMark

ARTICLES YOU MAY BE INTERESTED IN

Photodetachment spectroscopy of cold trapped NH_2^- near threshold
The Journal of Chemical Physics **149**, 104302 (2018); https://doi.org/10.1063/1.5042621

Photochemistry and spectroscopy of small hydrated magnesium clusters $Mg^+(H_2O)_n$, n = 1-5
The Journal of Chemical Physics **149**, 044309 (2018); https://doi.org/10.1063/1.5037401

Nucleophilic substitution with two reactive centers: The CN^- + CH_3I case
The Journal of Chemical Physics **143**, 184309 (2015); https://doi.org/10.1063/1.4934993

Lock-in Amplifiers up to 600 MHz
starting at $6,210


Zurich Instruments
Watch the Video

AIP Publishing

© 2018 Author(s).

NH_2^- in a cold ion trap with He buffer gas: *Ab initio* quantum modeling of the interaction potential and of state-changing multichannel dynamics

Mario Hernández Vera,[1] Ersin Yurtsever,[2] Roland Wester,[1] and Franco A. Gianturco[1,a)]
[1]*Institut für Ionenphysik und Angewandte Physik, Universität Innsbruck, Technikerstr. 25/3, A-6020 Innsbruck, Austria*
[2]*Department of Chemistry, Koç University, Rumelifeneriyolu, Sariyer TR-34450, Istanbul, Turkey*

(Received 17 January 2018; accepted 20 April 2018; published online 9 May 2018)

We present an extensive range of accurate *ab initio* calculations, which map in detail the spatial electronic potential energy surface that describes the interaction between the molecular anion NH_2^- ($^1A_1$) in its ground electronic state and the He atom. The time-independent close-coupling method is employed to generate the corresponding rotationally inelastic cross sections, and then the state-changing rates over a range of temperatures from 10 to 30 K, which is expected to realistically represent the experimental trapping conditions for this ion in a radio frequency ion trap filled with helium buffer gas. The overall evolutionary kinetics of the rotational level population involving the molecular anion in the cold trap is also modelled during a photodetachment experiment and analyzed using the computed rates. The present results clearly indicate the possibility of selectively detecting differences in behavior between the *ortho*- and *para*-anions undergoing photodetachment in the trap. © *2018 Author(s). All article content, except where otherwise noted, is licensed under a Creative Commons Attribution (CC BY) license (http://creativecommons.org/licenses/by/4.0/).* https://doi.org/10.1063/1.5022633

I. INTRODUCTION

The outstanding progress which has been made in recent years in preparing atoms and molecules, neutral and ionized, into confined environments with temperatures down to the nanokelvin domain has allowed the making of a very versatile toolbox to the instrumentation for investigating atomic and molecular processes with neutral and ionized species. In fact, trapped ions represent a highly controllable quantum system involving strong long-range Coulomb interaction.[1–3] Coulomb crystals of several ions where one can fully control their motion and their internal degrees of freedom are now available and indicate the potential for producing even larger systems in the future. There is indeed much still to be done in this area: from the creation of Coulomb crystals for a variety of polar molecules[4] to the laboratory study of the structure of astrophysical cold collisional processes and from quantum logic applications,[5] to ultraprecise atomic clocks,[6] to the ever-present desire to be able to control low-temperature chemical processes.[7] Thus, the development of these new techniques and their rapid application to increasingly newer systems has produced a continuing harvest of novel scientific findings.

In the present work, we shall be looking at a specific molecular anion, the closed shell $NH_2^-(^1A_1)$ system, which can be confined and internally cooled in ion traps by He as the buffer gas and further selectively "manipulated" by laser photodetachment processes. Buffer gas cooling uses a helium refrigerator to first cool He atoms which in turn cools the trapped molecular ions. Thus, the buffer gas is employed to dissipate translational energy of the partner molecule and, most important for our present analysis, the molecular internal rotational energy as well.[8] Hence, the buffer gas loading method relies on both elastic and inelastic collisions occurring in the ion traps to guide the trapped molecules to a lower temperature regime.

From the point of view of the theoretical and computational modeling of this process, several aspects of it need to be investigated and properly treated in order to bring to fruition the final interaction with the experiments done on the trapped ion by further laser interrogation: in the present instance, the expected experimental process is the state-selected photodetachment of the extra electron of the anion. The $NH_2(^2B_1)$ neutral partner turns out to have a positive electron affinity (EA) which we have calculated to be around 0.7 eV and, therefore, the formed anion $NH_2^-(^1A_1)$ is energetically more stable than its neutral counterpart. We shall further show below that, due to the localization of the excess electron into the π-type molecular orbital [highest occupied molecular orbital (HOMO)], its charge will have little effect on molecular geometries so that both molecules, neutral and anion, are structurally very close to each other with very similar vibrational and rotational structures.

If we therefore intend to realistically analyze the molecular internal state preparation by He gas uploading into the trap, we need to have first reliable knowledge of the He interaction with the partner molecule and then use it within a quantum dynamical treatment that generates the necessary state-to-state integral inelastic cross sections. The ensuing analysis of these

a)Author to whom correspondence should be addressed: francesco.gianturco@uibk.ac.at.

 © Author(s) 2018

cross sections to obtain the corresponding rotationally inelastic rate coefficients at the expected trap temperatures (i.e., from 10 to 30 K) will then allow us to produce the time-dependent evolution of the rotational state population of the trapped anions and thus detect the possible differences in the relative abundances of the spin isomers which are undergoing photodetachment in the trap.

In the following, we shall first discuss in detail the spatial strength of the potential energy surface (PES) of the interaction forces between NH_2^- and the He atom: this will be done in Sec. II. Section III will in turn report the state-to-state quantum calculations of the partial integral cross sections (ICSs) and the inelastic rate coefficients expected to be relevant for the trap temperatures of interest. In Sec. IV, we shall present the numerical solutions of the kinetic equations that will allow us to analyze the evolution of the rotational level populations and the relative abundances of both spin isomers of NH_2^- under the action of a photodetachment process in the trap. This analysis will help us to make specific suggestions about the most likely molecular ion states which can be prepared for the photodetachment experiments, currently carried out in our laboratory. Our present conclusions will be summarized in Sec. V.

II. ANISOTROPIC INTERACTION OF NH_2^-–He

The full 3D intermolecular interaction between the $NH_2^-(^1A_1)$ atom and the $He(^1S)$ atom is needed to carry out any quantum dynamics involving state-changing processes between the rotational states of the asymmetric rotor. We have therefore computed an accurate PES over the (R, θ, ϕ) grid defined within the reference frame reported in Fig. 1. This frame has its origin in the center of mass of the molecule, and its axes coincide with the principal axis of inertia of the NH_2^- partner.

We have selected a (θ, ϕ) grid of points over a series of spherical surfaces defined at each R values and then changed the radial variable over a range of distances that varied from 4.4 a_0 to 20.0 a_0. The initial grid of *ab initio* points (θ, ϕ) was formed by varying θ and ϕ in steps of 15°. Due to the symmetry of the 3D interaction, we should only have to consider the region of space within $0° \le \theta \le 90°$ and within $0° \le \phi \le 180°$.

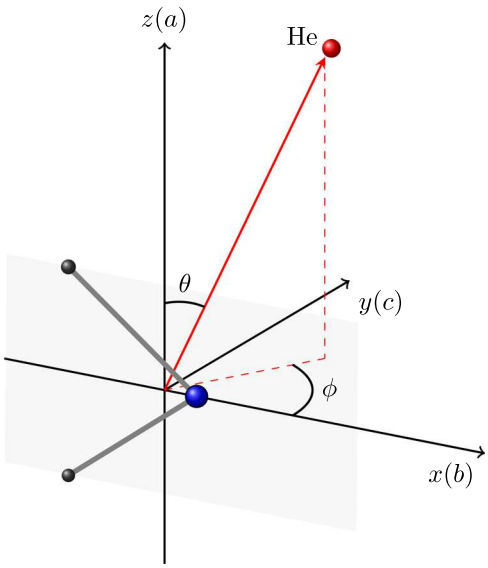


FIG. 1. Body-fixed frame of Cartesian coordinates for the $HeNH_2^-$ system. The anion is on the zx plane, and the x axis coincides with its principal axis of symmetry. The origin of the frame resides on the center of mass of NH_2^-, and it is very close to the N atom. Spherical coordinates describe the position of the He partner with respect to the asymmetric top molecular anion.

The calculations were carried out via the suite of codes provided by the MOLPRO package.[9] The level of post-Hartree-Fock (HF) treatment was at the coupled-cluster single double and perturbative triple [CCSD(T)] with a complete basis-set extrapolation starting from aug-cc-p-VXZ where X was chosen to be from triple (T), quadrupole (Q), and quintuple (5) successively. The HF energy was taken to be the one of the largest basis set, while the correlation energy was extrapolated using the n^{-3} functional form. We have also computed the electron affinity (EA) of the neutral $NH_2(X^2B_1)$ molecule, together with the optimized geometries of both the neutral and ionic partners. Such calculations were carried out at the CCSD(T)/aug-cc-pVQZ level of correlation. The present molecule has a positive EA with a value not too far from a fairly old experiment[10] (which yielded 0.71 eV) of 0.77 eV, indicating a rather stable anionic species. Furthermore, our present calculations indicate very little changes of the molecular geometry as one moves from the neutral to the anion. The H–N–H angle in fact changes from 102.9° in NH_2^- to 101.9° in NH_2^-, whereas the N–H distance changes from 1.0254 Å^2 in the neutral to 1.0290 Å^2 in the anion. Thus the Zero-point Energy (ZPE) correction to the EA value is negligibly small, and one expects very large Franck-Condon factors for any photodetachment process initiated by any NH_2^- (v = 0, j) selected state. One should further note the closeness of the structural values obtained by the present calculations and those provided by experiments.[11]

Since both molecules are polar species, it is important in future photodetachment simulations to know the permanent dipole moment and the dipole orientation in the initial anionic partner. We have calculated it for $NH_2^-(^1A_1)$ using the Hartree-Fock (HF) approach within the aug-cc-pVTZ expansion. The latter result turned out to be the same as that obtained by using a post-HF CCSD treatment. Hence, at the CCSD level of correlation, we found the same value of 1.4965 D. The orientation of the permanent dipole coincides with the direction of the unitary vector $\hat{\mathbf{x}}$ (see Fig. 1).

Another interesting piece of information obtainable from our calculations is linked to the spatial location of the bound excess electron in the negative ion since we already know that He atoms exhibit largely repulsive interactions with excess negative charges in the partner molecule. The bound additional electron is located in a double occupied π^* orbital directed along the y-axis of Fig. 1. The molecular plane is defined as the zx plane in the figure. A 3D view of that orbital is given in Fig. 2. That figure clearly shows the π^* orbital to be located on the nitrogen atom and perpendicular to the molecular plane.

To get a more specific view of the differences in the PES's strength as the (θ, ϕ) polar angles are changed, we show in Fig. 3 the behavior of the interaction as the radial distance changes along different approaches. The following comments could be made from a perusal of the data reported in that figure:

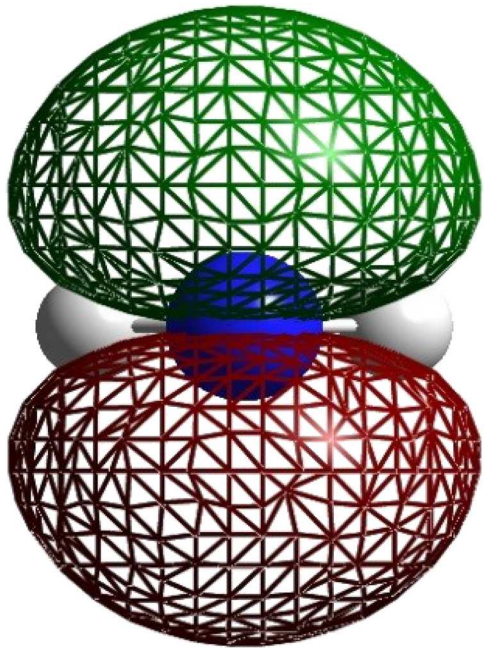


FIG. 2. Spatial extent of the highest occupied molecular orbital (HOMO) in the $NH_2^-(^1A_1)$. The N atom is located on the plane of the figure, while the two H atoms are shown in the same plane but away from the N atom and into the page. The isovalue chosen has been 0.05, as defined in the software Gaussview 5.0.8.

(i) The most repulsive interaction is shown to be the curve at $\theta = 90°$ and $\phi = 90°$ which corresponds to the He approach perpendicular to the molecule plane and toward the π^* region located on the N-atom. This is to be expected given the nature of the He interaction with negative charges.

(ii) A slightly stronger interaction is shown by the projectile's approach for $\theta = 90°$ and $\phi = 180°$. It corresponds to a trajectory on the molecular plane and on the side of two H atoms along the negative direction of the x-axis. This is also expected because of the small polarizability of the two hydrogen atoms and the overall repulsion generated by their nuclear location.

(iii) As is to be expected, the region of charges surrounding the N-atoms is more susceptible to be polarized by the incoming He atom since the distribution of the bound lone-pairs corresponds to more diffuse electron density values around that atom. Hence, the ($\theta = 90°$, $\phi = 0°$) direction describes a line of approach along the positive x-axis, directly hitting the N atom. With the same token, the ($\theta = 0°$, $\phi = 0°$) direction gives rise to the strongest attraction of the He atom by the molecular anion: it corresponds to approaching the nitrogen charge distribution along the positive z-axis, also in the molecular plane.

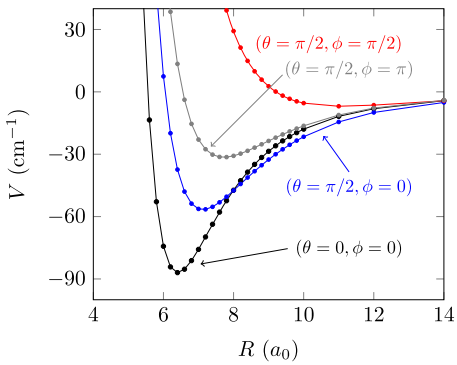


FIG. 3. Strength of the interaction potential along the radial coordinate and for different values of the (θ, ϕ) angles.

The above findings suggest that, in qualitative terms, we can expect the strongest region of interaction to be mostly on the molecular plane and also to be strongly dependent on the direction of approach. Such behavior is indicative of a PES which is markedly anisotropic and which shows very different strength of interaction depending on the region of approach to the molecule. This behavior is clearly presented in the panels of Fig. 4.

In both panels, one sees very clearly the strong repulsive region of interaction located around ($\theta = \phi = 90°$), i.e., directly on the y-axis and perpendicular to the molecule at the location of the π^* excess electron on the nitrogen atom. One can further see in both panels the presence of marked regions of attractive interaction for $\phi = 0°$ and θ being both around 0° and 180°. Such regions correspond to the He atom approaching the molecule along the positive and negative direction of the z-axis. With the same token, we also see a region of repulsive interaction at the shortest distance of the left panel of Fig. 4 close to $\phi = 180°$ and around $\theta = 90°$: it is the He

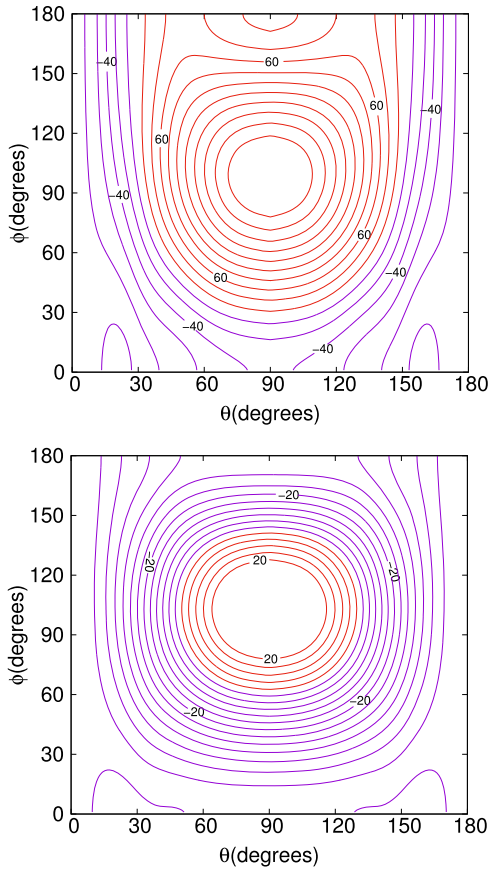


FIG. 4. Contour plots of the PES (in cm^{-1}) in polar coordinates at two fixed values of the R variable. Left panel: $R = 6.4\ a_0$ with contour lines equally spaced by 20 cm^{-1}; right panel: $R = 8.2\ a_0$ with contour lines equally spaced by 4 cm^{-1}. The blue lines correspond to the attractive regions, while the red lines show the repulsive regions.

approach along the x-axis toward the hydrogen atoms' side. This region becomes attractive when the fragments separate from each other by about $R = 5.0\ a_0$, as can be observed in Fig. 3.

On the whole, therefore, we can say that the present PES shows strongly attractive features which are typical of ionic interactions and further shows a marked anisotropy that will make it more efficient for the He atom to induce rotational transitions in the target rotor during the interaction with $NH_2^-(^1A_1)$. More details on this anisotropy-driven inelasticity of rotational state-changing collisions will be further discussed in Sec. III.

In order to implement the scattering calculations, the PES is conveniently expressed in terms of spherical harmonics.[12] Using the same geometrical convention as in Fig. 1, the expansion is written as follows:

$$V(R,\theta,\phi) = \sum_{\lambda,\mu} v_{\lambda,\mu}(R)(1+\delta_{\mu,0})^{-1} \times [Y_{\lambda,\mu}(\theta,\phi) + (-1)^{\mu} Y_{\lambda,\mu}(\theta,\phi)]. \quad (1)$$

In the above expansion, only terms with even integer values of $\lambda + \mu$ are nonzero because of the symmetry of the molecule and the selection we have made for the axis. In our case, the principal C_2 symmetric axis is the x axis instead of the z axis. We have chosen the I^r convention[13,14] that differs from the traditional convention of Green and co-workers.[15] The principal advantage of our convention is that the matrix of the terms of the rotational Hamiltonian of the asymmetric top (see Sec. III) will be a more diagonal-dominated matrix.

Equation (1) can be inverted[16] to generate the $v_{\lambda,\mu}$ coefficients which provide the information of the He–NH_2^- interaction anisotropy to be employed in the scattering equations. We have constructed from the *ab initio* points a smooth 2D PES over the (ϕ, θ) spheres defined, as discussed earlier, for each *ab initio* value of R by using the Reproducing Kernel Hilbert Space (RKHS) method.[17] Then, the coefficients $v_{\lambda,\mu}$ were computed by integration in spherical coordinates using a Gauss-Legendre quadrature grid of 45 points in θ and a regular grid of 360 points in ϕ. The integration provides a new grid of $v_{\lambda,\mu}(R_i)$ that can be interpolated and extrapolated by applying once again the RKHS method for one dimension.

Figure 5 shows the strength of the different radial coefficients in the expansion given by the expression (1) in the repulsive and intermediate range of the potential interaction.

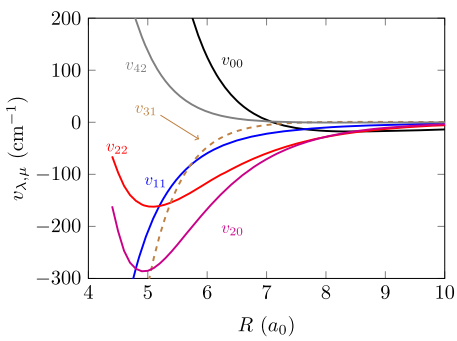


FIG. 5. Intermolecular distance dependence of the radial coefficients of the PES's expansion given by Eq. (1).

As we can see from that figure, the dominant terms at low collision energies correspond to the v_{20} and v_{22} terms. However, for higher collision energies, the term v_{11} contributes considerably to the shape of the PES and therefore to the collisional torque acting on the molecular rotor.

The long-range (LR) behavior of the global PES can be taken into account by a proper extrapolation of the $v_{\lambda,\mu}(R)$ coefficients. The LR interaction problem between He and NH_2^- is formulated and implemented via standard perturbation theory.[18] Because the He(^{1}S) partner does not contain any permanent moment, the first-order perturbed energy (electrostatic energy) of the system is zero. Therefore, for the present system, the induction energy is the one driving the asymptotic behavior of the potential. If we develop that energy in the multipole series and then match the corresponding terms with the expansion (1), we can determine the exponential law for the different radial coefficients for large values of R. For example, these considerations allow us to make the following comments about the dominant terms of the LR expansion:

(i) the strongest interaction in the asymptotic region is driven by the $v_{00} \approx C_4^{ind}/R^4$ contribution;
(ii) the $(\lambda = 1,\ \mu = 1)$ term corresponds asymptotically to the interaction of the molecular dipole with the polarizability of He via the term $v_{11} \approx C_5^{ind}/R^5$;
(iii) the $(\lambda = 2,\ \mu = 0)$ term also shows an attractive behavior and is asymptotically driven by the quadrupole interaction contribution $v_{20} \approx C_6^{ind}/R^6$.

Then the complete 3D surface can be generated by additionally introducing the radial coefficients in the expansion (1) with the appropriate extrapolation procedure. We have done this for the leading $\lambda = 0, 1, 2$ terms of the present PES which are, as shown earlier, the dominant terms at the low collision energies of interest here. The extrapolations were carried out by including in the RKHS fitting the radial kernels of the forms $q^{2,4}$, $q^{2,5}$, and $q^{2,6}$, respectively.

III. SCATTERING CALCULATIONS

A. Inelastic cross sections

Before presenting the results of the scattering calculations, it is convenient to briefly review how the rigid asymmetric top wave functions are defined and how their internal rotational energies are computed. To describe the energies and the wave functions of NH_2^-, one needs to first introduce the space-fixed (SF) frame and the body-fixed (BF) frame of reference, both with their origin in the center of mass of the anion. The axes of the BF frame coincide with the principal axes of the molecule (a, b, c), as is defined in Fig. 1. Following the I^r convention,[13] the Hamiltonian for the asymmetric top is defined by

$$\hat{H}_{rot} = \hbar^2 \Big\{ [(B+C)/2]\hat{\mathbf{j}}^2 + [A-(B+C)/2]\hat{j}_z^{\,2} + [(B-C)/4]\Big[(\hat{j}_m^+)^2 + (\hat{j}_m^-)^2\Big]\Big\}, \quad (2)$$

where A, B, and C are the rotational constants of the molecule associated with principal axes $z(a)$, $x(b)$, and $y(c)$ of the BF frame, $\hat{\mathbf{j}}$ is the total angular momentum operator, and $\hat{j}_m^+$ and $\hat{j}_m^-$ are the ladder operators for the eigenfunctions of $\hat{j}_z$. In order to compute the eigenstates and eigenvalues of the above

Hamiltonian, the asymmetric top wave functions are expanded onto a basis of symmetric top $|j, k_a, m\rangle$ wave functions. As usual, m denotes the projection of $\hat{\mathbf{j}}$ on the Z axis of the SF frame, and under the I^r convention, the k_a quantum number characterizes the projection of the total angular momentum on the $z(a)$ axis of the BF frame. The only nonvanishing matrix elements of $\hat{H}_{rot}$ in the basis of the symmetric top wave functions are those between states with the same j and m quantum numbers and between states having the same k_a values or k_a values differing by two. Furthermore, it is more convenient to work with symmetric top eigenfunctions with proper parity that can be defined as follows:

$$|j, k_a, m, \epsilon\rangle = [2(1+\delta_{\kappa 0})]^{-\frac{1}{2}}(|j, k_a, m\rangle + \epsilon|j, -k_a, m\rangle),$$

where $\kappa \geq 0$ and $\epsilon \pm 1$, excluding $\kappa = 0$ for which only $\epsilon = +1$ is allowed.

For each m and j quantum numbers, the matrix form of the Hamiltonian (2) can be block diagonalized into four blocks called E^+, E^-, O^+, and O^- depending on whether k_a is an even or odd integer and on whether ϵ is positive or negative.

The solution of the matrix form of the Schrödinger equation defined by Hamiltonian (2) for each value of j and one arbitrary value of m (i.e., $m = 0$) is therefore obtained by solving four systems of equations corresponding to each of the four blocks indicated above. Once the energies and the wave functions of the asymmetric top are computed, they can be associated by correlation with the energy labels of the *prolate* and the *oblate* limits, i.e., K_a and K_c. Sometimes it is also useful to define the additional label $\tau = K_a - K_c$, which runs from $\tau = -J$ to $\tau = +J$ in the order of ascending energy. Using the above notation, the asymmetric top wave functions are usually written in the following form:

$$\phi_\tau^{jm_j} = \sum_{k=0(1)}^{even(odd)} a_{k\tau}^j |j, k_a, m, \epsilon\rangle.$$

In addition, we should also take into account the fact that the NH_2^- can only exist either in the form of the para (p-NH_2^-) or the ortho (o-NH_2^-) spin isomers. To understand the distinction between the rotational levels for each spin isomer, we need to know how the exchange of the identical protons modifies the asymmetric rotational wave functions. In the C_{2v} symmetric group of the NH_2^- molecule, the exchange of proton is equivalent to a rotation of 180° about the b principal axis (see Fig. 1). This rotation affects the rotational wave function ϕ_τ^{jm} of the asymmetric top in the following way:[13]

$$R_b^\pi \phi_\tau^{jm} = \epsilon(-1)^j \phi_\tau^{jm}. \quad (3)$$

Therefore the p-NH_2^- energy levels are associated with positive blocks (E^+ and O^+) formed by $\epsilon = +1$ basis functions and even integer values of j, or with negative blocks (E^- and O^-) formed by $\epsilon = -1$ basis functions and odd integer values of j. For o-NH_2^-, the inverse relationship holds. The above rules also affect the labeling of the asymmetric top in terms of the total angular momentum and the prolate-limit body-frame projection quantum numbers. The $K_a = 0$ levels are associated with even values of j for p-NH_2^- and with odd values of j for o-NH_2^-. For $K_a \neq 0$, all possible values of j, except $j = 0$, are present for both spin isomers. The upper level of the pair with the same K_a and even j corresponds to the para permutation symmetry, while for odd values of j the upper level corresponds to the ortho permutation symmetry. The asymmetry splitting between both spin isomers becomes more marked as K_a decreases and j increases. These features are illustrated in Fig. 6.

We should be mindful of the fact that during the present ion—neutral inelastic collisions—the nuclear spins are only spectators because the magnetic interaction between the fragments can be neglected. Therefore the ortho-to-para conversion between molecular states is forbidden during the scattering processes we consider here. For this reason, we have to separately study the scattering dynamics of both spin isomers.

The partial integral cross sections (ICSs) describing the state-to-state rotational excitations of NH_2^- by collision with He were computed by using the HIBRIDON code.[19] The rotational constants A = 23.051, B = 13.067, and C = 8.121 in units of cm^{-1} were taken from the experimental values.[11] We have performed calculations over a range of total energies (E) from 0.2 to 760 cm^{-1} and from 21.3 cm^{-1} to 770 cm^{-1} for p-NH_2^- + He and o-NH_2^- + He collisional systems, respectively. The ICSs were computed over a grid of energies with steps of 0.2 cm^{-1} for $E < 270$ cm^{-1} and steps of 1 cm^{-1} for $E > 270$ cm^{-1} for both spin isomers. In all calculations, the outward integration was started in the classically forbidden region at 4.0 a_0. We have used two integrators to solve the standard time-independent coupled equations; for initial kinetic energies larger than 10 cm^{-1}, we used the log derivative integrator[20] from 4.0 a_0 to 30 a_0, while the Airy integrator[21] was employed from 30 a_0 up to 100 a_0. To avoid convergence problems of the ICS at low kinetic energies ($E_k < 10$ cm^{-1}) and for the larger values of the atom-anion relative angular momentum, the integration was extended up to 100 a_0 with the log-derivative integrator and from 100 a_0 to 500 a_0 with the Airy integrator. The final integral cross sections were computed by summing the partial contributions to the cross sections over a sufficiently large number of values of the total angular momentum J. At

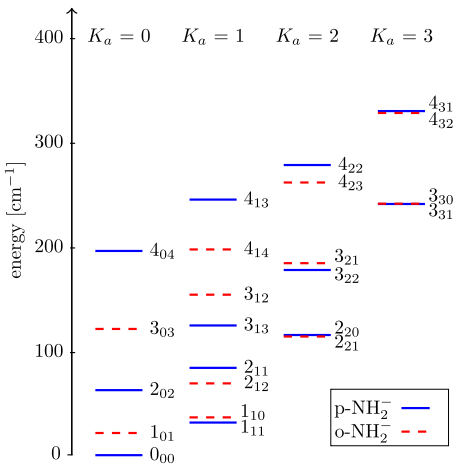


FIG. 6. Energy levels of p-NH_2^- (solid blue lines) and o-NH_2^- (dashed red lines) for the first 12 rotational states of both spin isomers. The vertical axis gives information about the rotational energies and the energy gaps. Each column is associated with a different value of the prolate-limit body-frame projection quantum number K_a.

the maximum total energy values, the J contributions were extended up to 100. Finally, we have performed all calculations including all angular basis functions with j up to $j = 7$. This has allowed us to reach convergence of the final cross sections with less than 2% of relative errors for all the dominant collision-induced transitions (ICS > 10^{-4} Å^2) between the first 7 rotational states of p-NH_2^- and o-NH_2^-. Finally, the implementation of the potential as given by the expansion (1) was truncated at $\lambda_{max} = 8$ and $\mu_{max} = 4$. Convergence tests have shown that further increasing the above parameters does not change the final numerical results.

The energy differences between the two sets of internal states of p-NH_2^- and o-NH_2^- molecular partners certainly appear to cause differences between the values of the ICS calculated among the rotational states of each spin isomer. The different panels of Fig. 7 show some of our computed ICS values for both spin states of the anionic partner. We can see in all panels that for low kinetic collision energies (e.g., up to about 10 cm^{-1}) the ICSs clearly exhibit many resonances associated with either the presence of closed channels forming metastable states of the complexes or with open-channel shape resonances due to the contributions of centrifugal barriers. These resonances can cause large variations of the ICSs, but to study them in some detail is, for now, outside the scope of our present analysis. The inset of Fig. 7(d) shows as an example the form of such resonances for the transition $1_{01} \rightarrow 2_{21}$ of the o-NH_2^-.

Figures 7(a) and 7(b) specifically present some transitions out of the states $|2_{20}\rangle$ of p-NH_2^- and $|2_{21}\rangle$ of o-NH_2^- toward the first 5 rotational states of both spin isomers. These initial states are very close in energy, as can be appreciated from the pictorial view reported in Fig. 6. For ortho and para spin modifications, the largest transitions are associated with $\Delta j = 0$, and, as a general propensity rule, the magnitude of the ICSs drops as the energy gap between the corresponding rotational levels increases. The above behavior has been also observed in rotational excitations of neutral asymmetric top molecular partners in collisions with He.[22] Another similarity between both spin modifications species is that the ICS can differ by orders of magnitude at low collision energies, but the differences between them gradually decrease as the kinetic energy rises to our largest values.

Useful information can also be extracted from the analysis of the computed inelastic ICS out of the ground rotational state of both p-NH_2^- and o-NH_2^-, as depicted in Figs. 7(c) and 7(d). In the case of p-NH_2^-, one of the dominant transitions occurs between the first two lower rotational states, i.e., 0_{00} and 1_{11}. These two rotational states are pure symmetric top wave functions, and their collisional interaction is directly connected by the v_{11} term of the potential. Because of the involved energy threshold, this transition cannot be accessed at low kinetic energies, but as the energy increases the dominant transition becomes $0_{00} \rightarrow 2_{02}$. The energy gap between 0_{00} and 2_{02} is larger, but the potential strongly couples these two rotational levels directly through the v_{20} term, which is one of the dominant terms of the potential expansion.

The most significant difference that we can appreciate from Figs. 7(c) and 7(d) is that at low collision energies, the ICS associated with the transition $1_{01} \rightarrow 1_{10}$ corresponding to ortho molecular states is by a factor of 2 larger than the ICS for the transition $0_{00} \rightarrow 1_{11}$ that corresponds to the para state of the molecular target. The $1_{01} \rightarrow 1_{10}$ cross section increases as the collision energy drops until it reaches a maximum value above 20 cm^{-1} in contrast to the $0_{00} \rightarrow 1_{11}$ cross section that uniformly decreases as the kinetic energy of the fragments decreases. Both transitions are directly coupled via the potential by the same v_{11} multipolar term, but the energy gap between the states of the ortho spin isomer is significantly smaller than

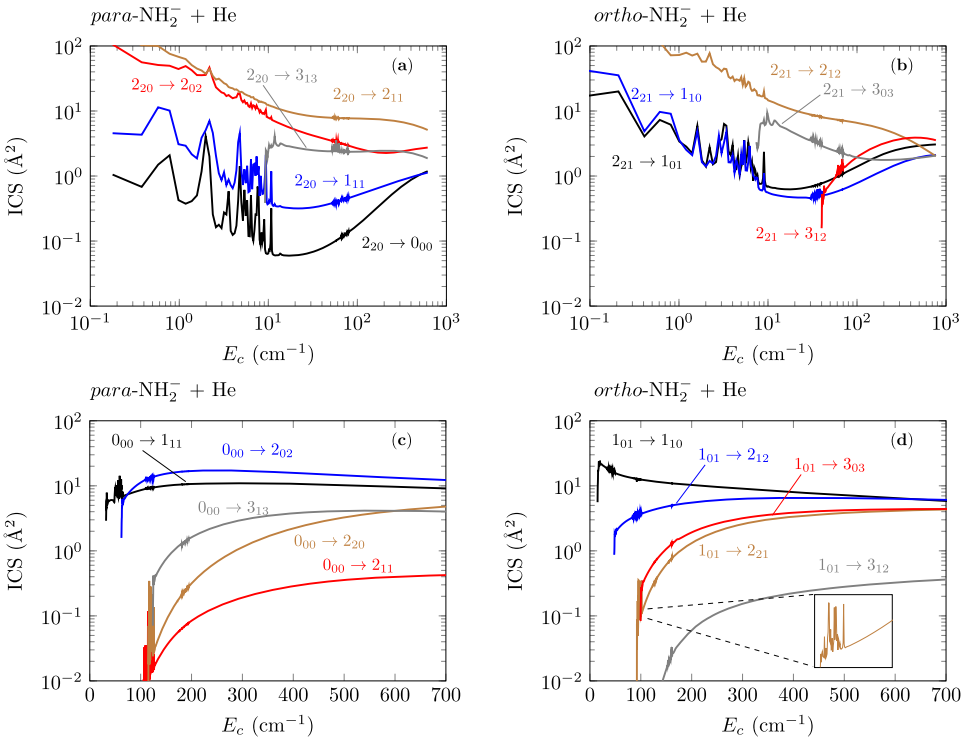


FIG. 7. Kinetic energy dependence of the integral cross sections for both spin isomer collisional systems. (a) Collision-induced transitions from the 2_{20} rotational state toward the first five rotational states of p-NH_2^-. (b) The same as before but for the initial 2_{21} rotational state of o-NH_2^-. (c) Rotational excitation transitions from the ground rotational state toward the first five rotational states of p-NH_2^-. (d) The same as (c) but for o-NH_2^-.

that for the para isomer. Such differences will play a significant role in the discussion of the results which we shall present in Sec. III B.

It is also interesting to note from Fig. 7(c) that the smallest cross section is associated with the transition $0_{00} \rightarrow 2_{11}$. This could be explained from the fact that the potential matrix elements between the states 0_{00} and 2_{11} are zero because of the absence of coupling terms in the potential when $\lambda + \mu$ takes odd values. The behavior of that cross section is therefore mainly driven by indirect potential couplings with other states included within the Coupled-Channel (CC) expansion.

A different picture arises for o-NH_2^-. In this case, the first four rotational levels are pure symmetric top wave functions. The maximum ICS at low kinetic energy corresponds to the $1_{01} \rightarrow 1_{10}$ inelastic transition, for which the initial and final states are only coupled by the term v_{11} of the potential expansion. However, at higher kinetic energies, the $1_{01} \rightarrow 2_{12}$ transition will include contributions from the couplings via the v_{11} and v_{31} terms, thereby dominating the inelastic process. We further see that the ICS of the $1_{01} \rightarrow 3_{03}$ inelastic transition, associated with the direct dynamical coupling via the v_{20} potential term, is not so large in this case because it is only at the higher collision energies that the odd values of lambda would be the dominant ones, as can be deduced from the observation of Fig. 5.

B. Inelastic rate coefficients

The rate coefficients $k(T)$ between different rotational states are computed from the cross sections by integration over the relevant range of collision energies. If we assume that the kinetic energy of both ions and neutral particles is given by a Boltzmann distribution in the ion trap, then the rate coefficient for the characteristic temperature T is given by the following expression:

$$k_{j_\tau \rightarrow j'_{\tau'}}(T) = \left(\frac{8}{\pi \mu k_B^3 T^3}\right)^{1/2} \int_0^\infty E_c \sigma_{j_\tau \rightarrow j'_{\tau'}}(E_c) e^{-E_c/k_B T} dE_c, \tag{4}$$

where σ is the cross section from the initial level j_τ to the final level $j'_{\tau'}$, μ is the reduced mass of the system, and k_B is Boltzmann's constant.

Figure 8 shows a subset of the inelastic scattering coefficients of p-NH_2^- and o-NH_2^-, describing the collisional relaxation among the first five rotational levels at 30 K. The differences in size between the rates pertaining to the two spin isomers can be clearly seen in that figure, especially for the transitions involving the first two excited states of each isomer species: they are those that will be active during the photodetachment process further described below. For both spin isomers, most of the transitions follow a similar rule, as already observed in Sec. III A: the rates between any two states increase as the energy gaps between such states decrease. This occurs for all transitions out of the states 2_{20}, 2_{11}, and 2_{02} of p-NH_2^- and for some transitions out of 3_{12}, 3_{21}, and 3_{12} of o-NH_2^-. Some exceptions to such a rule can be explained in terms of differences between the relative strengths of the involved potential couplings. For example, the transition $3_{13} \rightarrow 2_{02}$ is more likely to occur than the transition $3_{13} \rightarrow 2_{20}$

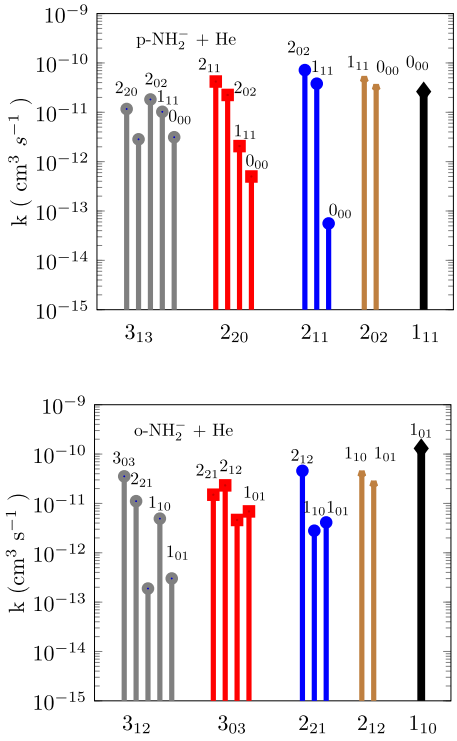


FIG. 8. Inelastic rate coefficients describing the collisional relaxation at 30 K from the first five rotational states of p-NH_2^- and o-NH_2^-. The levels reported at the bottom of the figure indicate the initial quantum states, while the levels reported above the vertical "sticks" denote the final rotational states.

because in the first case the coupling, driven by the v_{11} term in the potential expansion, is stronger when connecting two symmetric top functions involving multiplication of large mixing coefficients $a^j_{k\tau}$ [see Eq. (3)] within the asymmetric top wave function expansion. One can also see in Fig. 8 that the largest values of the rate coefficients are associated with $\Delta j = 0$ transitions. The largest rate of p-NH_2^- corresponds to the $2_{11} \rightarrow 2_{02}$, while in the case of o-NH_2^-, the largest one corresponds to the transition $1_{10} \rightarrow 1_{01}$.

The most marked differences observed in Figs. 8(a) and 8(b) between the o-NH_2^- and p-NH_2^- rates are observed with the rotational relaxation processes among the first two excited rotational states in the two sets of systems. The same type of difference was already pointed out in Sec. III A when we described the excitation ICSs between these states so that the physical explanation is therefore the same one, i.e., linked to the differences in the transition energy gaps. In addition, using the detailed balance principle as a supporting proof, we can also surmise that the rates describing the excitation processes between the same levels will also be very different for each of the spin isomers.

In conclusion, we have seen from the above calculations that although the two spin isomers manifest some similarities in the behavior of their respective inelastic rate coefficients, there are also substantial differences derived from their different internal energy spacings within the relevant rotational states and from the different strengths of the dynamical couplings between each level as driven by the anisotropic potential interaction discussed earlier. Such differences should therefore affect the rotational level populations of the ions as they

collisionally evolve under the expected experimental conditions in the cold ion traps, where they are also undergoing photodetachment via laser depletion. In Sec. IV, we shall therefore present a fairly simple computational model that will illustrate this evolution under photodetachment experiments.

IV. ROTATIONAL POPULATION COLLISIONAL EVOLUTION

In order to gain more insight into the possible effects coming from some of the large differences observed among the relative sizes of the inelastic rate coefficients computed in Sec. III B for o-NH_2^- + He and p-NH_2^- + He collisional systems, respectively, we present in this section a fairly simple modeling that describes an "ideal" photodetachment experiment in the cold ion trap.

As it was recently demonstrated by the earlier work in our group,[23] it is possible to experimentally manipulate the rotational quantum states of a rigid rotor confined in a cold ion trap. The method, which can also be applied to the present problem, consists in depleting by an intense photodetachment laser the first excited states of each spin isomer while however leaving the ground state anions intact, as is illustrated in the scheme reported in Fig. 9. The change of the electronic symmetry from being $^1A_1$ in the anion to becoming $^2B_1$ in the neutral molecule causes a corresponding change in the rotational levels of the final product after the photodetachment step has taken place.

Both spin states of NH_2^- at low temperatures are relatively good representations of an asymmetric top molecule as neither electronic nor nuclear spin momentum couples appreciably to the mechanical rotation of the molecule. Therefore the rates computed in this work are also suitable to be further employed to solve the master equations that describe the evolutionary processes illustrated in Fig. 9.

We consider in the following work a simple modeling which assumes for the moment that the destruction rates of the photodetachment step are the same for both para- and ortho-spin modifications. The latter isomers, at this simpler picture of our modeling, are further taken to be of equal abundance within the ion trap. Additionally, we neglect for the moment

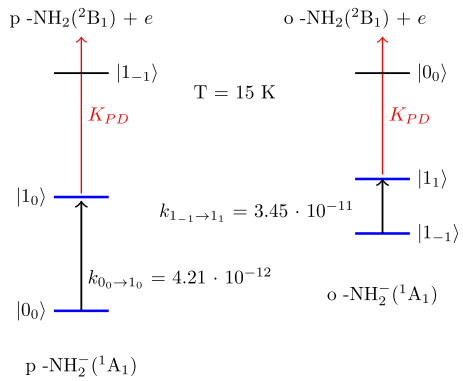


FIG. 9. Schematic representation of state-selective removal of negative ions by threshold photodetachment experiments. Here we have used the symbol $\tau = K_a - K_c$ to denote the different rotational states. The units of the rates for the presented transitions $k_{1_{-1}\to 1_1}$ and $k_{0_0\to 1_0}$ are (cm^3 s^{-1}). The temperature for which the rates are shown is 15 K.

any induced or spontaneous radiative dipole transitions in the anions. This choice is backed by the fact that, given the low density flux of the black-body radiation distributed in the trap, and the smallness of the Einstein coefficients found in general for the radiative emissions between the lower rotational levels of rigid rotors,[23] we do not expect that the radiative processes would be playing a crucial role for the present modeling of the photodetachment experiments.

We assume that the laser affects primarily the first and the second rotationally excited states of each spin isomer. Such assumptions are somewhat justified when one takes into account the existing selection rules for the transitions mentioned before and also the fact that the rotational states which are higher up in energy are not very populated at the trap temperatures we are considering. When using the above assumptions, the master equations describing the changes of rotational populations of the anions are given by the following expression:

$$\frac{dn_i(t)}{dt} = \sum_{j\neq i} n_j(t)C_{ji} - n_i(t)\sum_{j\neq i} P_{ij}, \tag{5}$$

where P_{ij}, the destruction rate coefficient of level i, and its formation rate coefficient C_{ji} are given by

$$P_{ij} = n_{\mathrm{He}}k_{i\to j} + K_{PD}, \tag{6}$$

$$C_{ji} = n_{\mathrm{He}}k_{j\to i}, \tag{7}$$

where K_{PD} (s^{-1}) is the destruction rate caused by the laser and n_{He} is the density of the He buffer gas. In the interval of time τ in which the laser is applied, the separate fractions of the ions that are lost for each isotopic species can be computed from the following expression:

$$F_{ions}(t_0+\tau) = \frac{\sum_i n_i(t_0+\tau)}{\sum_i n_i(t_0)}, \tag{8}$$

where t_0 is an initial interval of time necessary to bring the population of the rotational levels to the Boltzmann distribution associated with the temperature of the uploaded He buffer gas, after starting from arbitrary initial conditions for the rotational states of the molecular gas. If at the initial time the populations are normalized, it is clear that F_{ions} will be only less than one whenever the term K_{PD} is nonzero in the master equations, i.e., when the photodetaching laser beam is switched on.

We have numerically integrated Eq. (5) using a four order Runge-Kutta method employing the current rates at 15 K and for a density of 10^{10} cm^{-3} of the He buffer gas. The K_{PD} value was taken to be equal to 1 s^{-1}. This value was estimated from earlier experiments, but it can be clearly treated as a changeable parameter depending on the experimental conditions. However, this type of analysis will be done elsewhere, in further work currently being planned in our group, as it is beyond the scope of the present modeling.

We have also included in the master equation the transitions among the first 6 rotational states of the molecule. However, at such low temperatures, only the transitions between the first three rotational states of the ions will drive the solution of master equation because the higher rotational states are negligibly populated in our "thought experiment" and because

excitations with $\Delta j > 1$ are small due to the lack of availability of sufficient kinetic energy to drive the collisional transition. In order to reach the equilibrium, we first solve the equations for an interval of $t_0 = 15$ s considering that all the molecules are in their ground state at $t = 0$ and without including the term K_{FD}. Then, at 15 s, we include the term K_{FD} which describes the turning on of the population-depleting laser.

The upper panel of Fig. 10 shows the temporal evolution of the first 3 rotational states of both spin isomers over an interval of 5 s. As we can see, at the initial equilibrium regime, the ground state of *o*-NH_2^- is more populated at 15 K than the ground state of *p*-NH_2^-. However, the destruction of the ground state of this species, driven by the inelastic collisions, is much more efficient, as already shown by the size of the inelastic rate coefficient between the ground and the first excited states of the ortho modification reported before by Fig. 8. Hence, most of the molecules collisionally excited will be rapidly destroyed by the laser once they have reached their first excited state. The collision-induced transitions from the ground to the second excited rotational states are instead much slower because the second excited rotational states of both spin isomers are higher in energy (see Fig. 6) and therefore involve much larger energy gaps in the collisional transitions. Therefore, at 15 K, our calculations suggest that the destruction of the ions is mainly driven by the laser photodetachment rate, which is fast depleting the first excited states, and by the collisionally inelastic rate coefficient connecting the ground and that first excited rotational state. The above reasoning should therefore explain why the *o*-NH_2^- molecules are lost more rapidly than the *p*-NH_2^- isomers, as can be clearly appreciated from the present results given in the lower panel of Fig. 10.

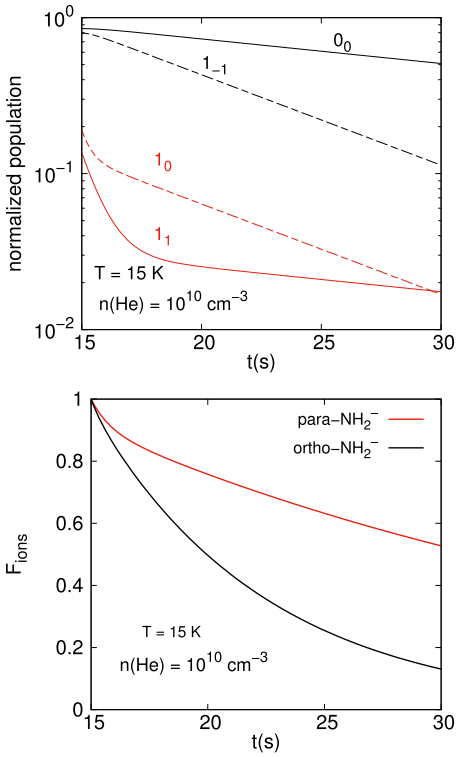


FIG. 10. Upper panel: Evolution of the rotational level population as a function of time, starting after 15 s and at 15 K corresponding to the numerical solution of the master equations. We have set a Boltzmann distribution as the initial condition of the rotational populations. Continuous lines and dashed lines denote the level population of *p*-NH_2^- and *o*-NH_2^-, respectively. Lower panel: Comparison of the relative losses of *p*-NH_2^- and *o*-NH_2^- in the ion trap for an ideal experiment, in which the photodetachment destruction rates are the same for both spin isomers. See the main text for further details.

The results presented here therefore suggest that the *p*-NH_2^- spin isomer will be more likely to survive in the trap and thus become more suitable for rate comparisons between theory and experiments at low temperatures. As Fig. 10 shows, the excited rotational states of the above isomer are depleted very fast by the laser action, although its ground rotational state remains more populated than the ortho variant since the latter leaves its ground state more quickly than the former, as indicated in the scheme of Fig. 9. This suggests that, after about 1 s, the exponential law that ultimately shall govern the destruction of this isomer is largely determined by the dominance of the rate $k_{0_0 \to 1_0}$, a consequence of the simplification of the master equations induced by the selective level populations into the trap driven by the initial collisional cooling rates.

If we now turn to the evolutionary behavior of *o*-NH_2^-, we see that, because of the smaller rotational energy spacings between its levels, the above reduction of the master equation to a single dominant rate is more difficult to achieve since several depletion rates will be similar in size and efficiency during the photodetachment process.

From the above analysis of the evolutionary behavior of the molecular populations with our fairly simple modeling, we can also conclude that the differences between the relative losses of the two spin isomers will become more significant if we were to explore lower temperatures within the trap since the relative differences in level populations will be more significant and involving a smaller number of states.

V. CONCLUSIONS

In the present work, we have computed, starting from an *ab initio* evaluation of a new anisotropic intermolecular potential energy surface, the collisionally inelastic cross sections and the ensuing rate coefficients for the He + NH_2^- collisional system. We have investigated in this study a range of collisional energies and temperatures which are typical of ion trap experiments, i.e., in the temperature region between about 10 K and 30 K. Our calculations were based on a new accurate PES, and the scattering calculations were performed employing the quantum Coupled-Channel (CC) method. The present results have shown that the rotational excitation of *p*-NH_2^- and *o*-NH_2^- driven by the inelastic collisions with He follows a series of propensity rules which are governed by the different potential couplings acting between the different rotational states and by the energy spacings between different rotational states. Such propensity rules are also responsible for the appearance of marked, and significant, differences between the behavior of the two spin isomers. For example, we have found that the rates at low temperatures between the ground and the first rotational states of both spin modifications are very large and larger than those shown between other rotational levels which we have examined. We have further endeavoured to illustrate, using a simple modeling of the kinetics conditions in an ideal cold trap, how the above differences between collisional rates could in

turn drive the preferential destruction of the ortho species with respect to the para ions during laser-induced photodetachment processes in cold trap experiments. Such a feature would certainly be amenable to verification by the ongoing experimental search carried out in our laboratory.

The present study is therefore able to provide specific and fairly realistic indicators for conducting such experiments involving the title anion in both its isomeric forms, collisionally cooled by He gas in the cold traps and selectively depleted by the action of a photodetaching laser beam.

SUPPLEMENTARY MATERIAL

See the supplementary material for the complete description of the electronic potential energy surface presented and discussed in the main text. The program "expansion" evaluates the fitting of the PES via an expansion in spherical harmonics. We have compiled the code with the Intel Fortran compiler [Intel(R) 64, Version 13.0.1.117]. The code will ask for the spherical coordinates of the point where the potential will be evaluated. The value of the potential is in units of cm^{-1} and is printed in the output. For more information about the definition of the coordinates, see Fig. 1 in the main text.

ACKNOWLEDGMENTS

F.A.G. and R.W. thank the Austrian Science Fund (FWF) for supporting the present research through Project No. P29558-N36. The support of the Computational Center of the University of Innsbruck is also acknowledged. We are grateful to Olga Lakhmanskaya and to Professor F. Lique for several discussions.

[1] W. Paul, Angew. Chem., Int. Ed. Engl. **29**, 739 (1990).
[2] R. Wester, J. Phys. B: At., Mol. Opt. Phys. **42**, 154001 (2009).
[3] S. Willitsch, Int. Rev. Phys. Chem. **31**, 175–199 (2012).
[4] M. Drewsen, A. Mortensen, R. Martinussen, P. Staanum, and J. L. Sørensen, Phys. Rev. Lett. **93**, 243201 (2004).
[5] J. I. Cirac and P. Zoller, Phys. Rev. Lett. **74**, 4091–4094 (1995).
[6] A. D. Ludlow, M. M. Boyd, J. Ye, E. Peik, and P. O. Schmidt, Rev. Mod. Phys. **87**, 637–701 (2015).
[7] A. Härter and J. H. Denschlag, Contemp. Phys. **55**, 33–45 (2014).
[8] J. M. Doyle, B. Friedrich, J. Kim, and D. Patterson, Phys. Rev. A **52**, R2515–R2518 (1995).
[9] H.-J. Werner, P. J. Knowles, G. Knizia, F. R. Manby, and M. Schuetz, Wiley Interdiscip. Rev.: Comput. Mol. Sci. **2**, 242–253 (2012).
[10] C. T. Wickham-Jones, K. M. Ervin, G. B. Ellison, and W. C. Lineberger, J. Chem. Phys. **91**, 2762–2763 (1989).
[11] L. M. Tack, N. H. Rosenbaum, J. C. Owrutsky, and R. J. Saykally, J. Chem. Phys. **84**, 7056–7057 (1986).
[12] B. J. Garrison, W. A. Lester, Jr., and W. H. Miller, J. Chem. Phys. **65**, 2193–2200 (1976).
[13] P. R. Bunker, *Molecular Symmetry and Spectroscopy*, 2nd ed. (NRC Research Press, 1998).
[14] P. J. Dagdigian and M. Alexander, Mol. Phys. **108**, 1159–1169 (2010).
[15] A. Palma, S. Green, D. J. DeFrees, and A. D. McLean, J. Chem. Phys. **89**, 1401–1407 (1988).
[16] T. V. Tscherbul, T. A. Grinev, H.-G. Yu, A. Dalgarno, J. Kłos, L. Ma, and M. H. Alexander, J. Chem. Phys. **137**, 104302 (2012).
[17] T. S. Ho and H. Rabitz, J. Chem. Phys. **104**, 2584–2597 (1996).
[18] A. D. Buckingham, *Advances in Chemical Physics* (John Wiley & Sons, Inc., 2007), pp. 107–142.
[19] The Hibridon package was written by M. H. Alexander *et. al.*, Copyright (c) 1987, 1991, 1993, 1996, 2000, 2001, 2003, 2004, 2007, 2008, 2009, 2010, 2011, University of Maryland at College Park. All rights reserved.
[20] D. E. Manolopoulos, J. Chem. Phys. **85**, 6425–6429 (1986).
[21] M. H. Alexander, J. Chem. Phys. **81**, 4510–4516 (1984).
[22] L. Ma, M. H. Alexander, and P. J. Dagdigian, J. Chem. Phys. **134**, 154307 (2011).
[23] D. Hauser, S. Lee, F. Carelli, S. Spieler, O. Lakhmanskaya, E. S. Endres, S. S. Kumar, F. Gianturco, and R. Wester, Nat. Phys. **11**, 467–470 (2015).